I&EC research
Industrial & Engineering Chemistry Research

Article

pubs.acs.org/IECR

Uniform Carbon Coating on Silicon Nanoparticles by Dynamic CVD Process for Electrochemical Lithium Storage

Jinglu Yu,[†] Jun Yang,[†,*] Xuejiao Feng,[†] Hao Jia,[†] Jiulin Wang,[†] and Wei Lu[‡]

[†]School of Chemistry and Chemical Engineering, Shanghai Jiao Tong University, Shanghai, 200240, China

[‡]Department of Mechanical Engineering, University of Michigan, Ann Arbor, Michigan 48109, United States

Supporting Information

ABSTRACT: A uniform carbon layer was coated on Si nanoparticles by the dynamic chemical vapor deposition (CVD) process with toluene as the carbon source. The carbon layer thickness could easily be adjusted by controlling the preparation conditions. Samples selected from different positions of the reaction tube showed a small deviation in carbon content. As an anode material for a lithium-ion battery, the resulting Si@C composites exhibited better cycle reversibility and rate capability than pristine Si. The Si@C-2 sample (carbon layer thickness ≈ 12 nm) delivered a relatively stable specific capacity of ca. 1600 mA h g^{-1} at 0.3 A g^{-1} for 70 cycles. Its capacity remained at 750 mA h g^{-1} at 5 A g^{-1}, compared with 240 mA h g^{-1} for pristine Si. Acetylene as a carbon source can also lead to superior cycle stability. This reformative CVD process provides an avenue for the large-scale production of uniform carbon coating materials used for batteries and other devices.

1. INTRODUCTION

With the rapid development of electric vehicles (EVs) and grid-scale energy storage systems, there are ever-increasing demands for lithium-ion batteries (LIBs) with high energy density and long cycle life.[1−3] Graphite, the traditional anode material in LIBs, cannot meet high energy needs because of its limited theoretical specific capacity of 370 mA h g^{-1} and poor rate capability.[4] Silicon as an anode material has prominent advantages, such as a high theoretical specific capacity of 4200 mA h g^{-1}, a fairly low discharge potential (~0.4 V versus Li^+/Li), and a rich resource, and it has recently attracted significant attention as the most promising candidate to replace graphite.[5−7] However, Si exhibits large volume changes (>300%) during lithiation−delithiation, which can cause cracking and pulverization in the electrode, leading to a loss of electrical contact and excessive growth of the solid−electrolyte interphase (SEI).[8−11] As a result, Si suffers from rapid capacity decay and a short cycle life.

Many efforts have been made to accommodate the volume changes of silicon, such as by preparing nanosized silicon-based materials (including nanowires,[12,13] nanotubes,[14−16] and nanoparticles[17,18]), porous silicon-based materials,[19,20] and silicon-active/-inactive composites.[21−23] Of all such approaches, the design of silicon/carbon composites has become an important research direction because of the good electronic conductivity and stress-buffer nature of carbon in improving the stability of silicon-based anodes.[22,24] In recent years, various methods have been employed for preparing silicon/carbon composites, such as a hydrothermal method,[25] chemical vapor deposition (CVD),[26,27] high-energy mechanical milling (HEMM),[28] spray drying,[21] pyrolysis,[29] and a sol−gel method.[30] The sol−gel method is not suitable for mass production, and mechanical milling seems unable to create a high-quality carbon layer. Compared with pyrolysis, CVD carbon coating can form a more uniform carbon layer on the Si surface with a controllable thickness and facile processing.[20] However, the uniformity of the carbon coating is poor in a conventional stationary CVD apparatus, especially for large amounts of samples. Yoshio et al.[31] prepared carbon-coated Si microparticles in large amounts by repeated CVD treatment to improve the carbon layer uniformity. The obtained material delivered a delithiation capacity of over 800 mA h g^{-1} after 20 cycles. Nevertheless, this process is relatively complicated, leading to low productivity. Another improved technology is pressure-pulsed CVD, in which reactant gas more easily penetrates into packed powder through repeated evacuation and gas feed.[32]

In this work, commercially available nanosized Si powder was employed. The Si nanoparticles were coated with a carbon nanolayer in a rotational CVD apparatus that is industrially scalable. The effects of the carbon layer thickness and carbon source on the electrochemical behavior, as well as the morphology evolution of the composite during cycling, were systematically examined.

2. EXPERIMENTAL SECTION

2.1. Preparation of Si@C Composite. The rotational CVD carbon coating machine used in the current study is available from Hefei Kejing Materials Technology Co., Ltd., and is schematically presented in Figure 1. First, 2 g of Si nanoparticles (50−200 nm, Alfa-Aesar) were placed in the center of the quartz tube furnace (represented in yellow in Figure 1). This central tube contains four blades (Figure S1, Supporting Information), and the tube was rotated at a set speed of 9 rpm to facilitate the movement of Si nanoparticles with a similar probability of exposure to vapor surroundings, leading to homogeneous carbon deposition. Second, the furnace temperature was increased from room temperature to

Received: March 11, 2014
Revised: July 21, 2014
Accepted: July 23, 2014
Published: July 23, 2014

dx.doi.org/10.1021/ie5010465 | Ind. Eng. Chem. Res. 2014, 53, 12697−12704

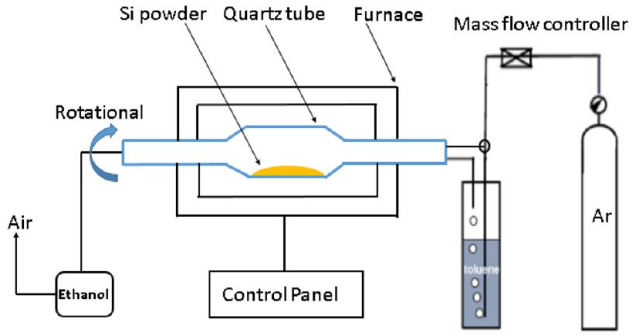

Figure 1. Schematic of the rotational CVD carbon coating system.

300 °C under pure argon atmosphere at a heating rate of 10 °C min^{-1}. Then, the precursor gas, namely, toluene plus argon (argon was bubbled through a toluene reservoir at a flux of 100 L h^{-1}), was introduced into the furnace, and the temperature was raised from 300 to 800 °C and held at 800 °C for a set time, unless specified otherwise. The toluene gas decomposed quickly at 800 °C, and carbon was deposited onto the surface of the Si particles. After the set time was reached, the toluene gas was stopped, and the argon gas was kept flowing in the furnace for 30 min at 800 °C to allow the toluene gas remaining in the furnace react completely. Finally, the furnace was cooled slowly in pure argon to room temperature, and the resulting composite Si@C was obtained. The set times at 800 °C were 1, 2, and 3 h, and the obtained samples are denoted as Si@C-1, Si@C-2, and Si@C-3, respectively. Acetylene as the carbon source was also investigated and compared. For the CVD process, the furnace temperature was increased from room temperature to 800 °C under a mixed gas of argon (150 mL min^{-1}) and acetylene (40 mL min^{-1}) at a heating rate of 15 °C min^{-1} and kept at 800 °C for 1.5 h for the CVD process. The resulting composite is designated as Si@C-ac.

2.2. Structural and Morphological Characterization. The powder samples were characterized by X-ray diffraction (XRD) using a Rigaku D/MAX-2200/PC X-ray diffractometer at 40 kV and 30 mA with a Cu Kα (λ = 1.54056 Å) radiation source (0.3-mm receiving slit, scintillation counter). Data were collected over the 2θ range from 10° to 80° at a scanning speed of 5° min^{-1} at ambient temperature. Raman spectroscopy was employed to identify the carbon structural characteristics of the carbon coating samples using a Thermo Scientific DXR Raman microscope as a laser wavelength of 532 nm at room temperature. The morphologies and microstructures of the composite materials were observed and characterized by field-emission scanning electron microscopy (FESEM, JEOL JSM-7401F) and transmission electron microscopy (TEM, JEOL JEM-100CX), respectively. The carbon weight fractions in Si@C samples were determined by evaluating the mass loss of Si@C composites after calcination by thermogravimetric analysis (TGA, TA 2050).

2.3. Electrochemical Measurements. The electrochemical performance of the as-prepared composites was evaluated using two-electrode coin-type cells. The working electrodes were prepared by pasting a mixture of the active material, Super P conductive carbon black (40 nm, Timcal) as an additive, and styrene butadiene rubber/sodium carboxymethyl cellulose (SBR/SCMC, 3:5 by weight, dissolved in distilled water) as a binder at a weight ratio of 60:20:20. After the mixture had been coated onto Cu foil, the electrodes were dried, cut into Φ12 mm disks, pressed at 3 MPa for 40 s, and finally dried at 50 °C in a vacuum for 4 h. The mass loading of the active Si@C material was ca. 0.6 mg cm^{-2}. The CR2016 coin cells were assembled in an argon-filled glovebox (MB-10 compact, MBraun) using an electrolyte solution of 1 M $LiPF_6$ in a dimethyl carbonate (DMC)/ethylene carbonate (EC) mixed solvent of 1:1 by volume, including 2 wt % vinylene carbonate (VC) as an electrolyte additive, a polyethylene (PE) membrane (Teklon UH2045.5) as a separator, and lithium metal as the counter electrode. The cycling performance was evaluated on a LAND battery test system (CT2007A, Wuhan Jinnuo Electronics, Ltd.) at 25 °C with constant current rates and a rest time of 5 min between charge and discharge. The charge and discharge current rates were equal for each test. The cell cutoff voltages were 0.01 and 1.2 V versus lithium counter electrode for discharge (Li insertion) and charge (Li extraction), respectively. The specific capacity and the current rate were calculated on the basis of the weight of Si@C composite.

3. RESULTS AND DISCUSSION

XRD patterns of the pristine Si powder and Si@C-2 are compared in Figure 2. Both samples exhibit highly crystalline

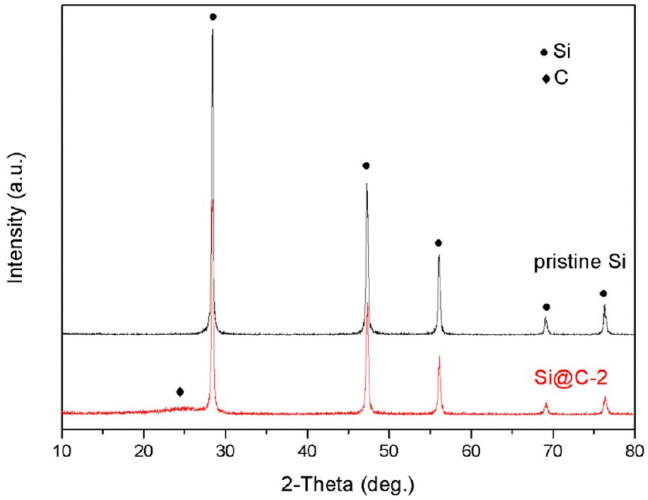

Figure 2. XRD patterns of pristine Si and Si@C-2.

structures that match well with the standard Si peaks (JCPDS 27-1402). The peaks at 28°, 47°, 56°, 69°, and 76° can be indexed as the (111), (220), (311), (400) and (331) planes, respectively, of Si crystals. For Si@C-2, there is an additional broad peak near 24° arising from the amorphous carbon. To quantify the amount of carbon in Si@C-1, Si@C-2, and Si@C-3, TGA was conducted at a heating rate of 20 °C min^{-1} from 40 to 800 °C in air (Figure 3), and TGA of the Si powder was also performed for comparison. For Si@C-1, Si@C-2, and Si@C-3, the rapid weight loss between ~600 and ~730 °C can be attributed to the combustion of carbon in the Si@C composites, and the slight increase in weight after ~730 °C is due to the formation of SiO_x. From these results, the weight fractions of carbon in Si@C-1, Si@C-2, and Si@C-3 were determined to be about 14.8%, 29.6%, and 42.4%, respectively. It is reasonable that the carbon content in the composites increased with the prolonged reaction time. TGA was further used to check homogeneity of the CVD carbon coating in six different positions in the furnace tube with 2 g of Si powder per batch (Figure S2, Supporting Information). It was found that

dx.doi.org/10.1021/ie5010465 | Ind. Eng. Chem. Res. 2014, 53, 12697−12704

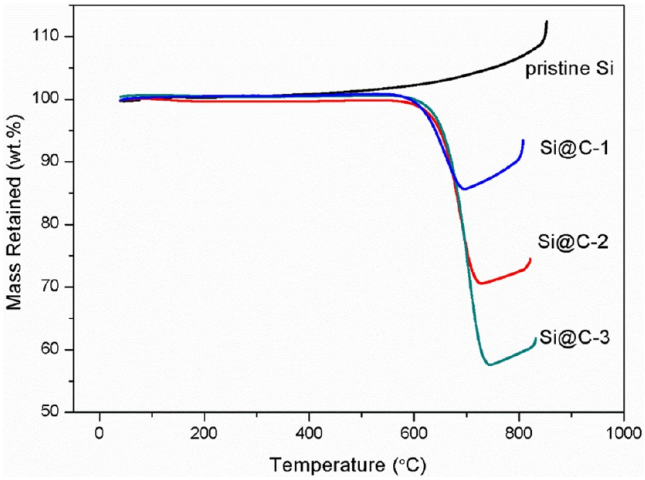

Figure 3. Thermogravimetry analysis of Si@C-1, Si@C-2, Si@C-3, and pristine Si.

the carbon contents of Si@C-2 from these positions were very similar, with a ±3% deviation, indicating that the carbon dispersion in the sample per batch was homogeneous. However, for a traditional stationary CVD process, an uneven carbon coating was observed even for only 0.6 g of Si powder per batch, where the upper part of the sample was gray whereas the bottom part was still yellow (not shown here).

As shown in Figure 4a,b, the particle size of Si powder ranged mostly from 50 to 200 nm, and the Si@C-2 particles became larger as a result of carbon deposition. The complete carbon coating layers on the Si particles can be clearly observed in Figure 4c. The microstructures and thicknesses of the carbon layers for various samples were further characterized by TEM (Figure 5). In Figure 5a, a SiO_x layer of 1−2 nm can be observed on the surface of a pure Si particle. The carbon layer thicknesses of Si@C-1, Si@C-2, and Si@C-3 were found to be ca. 7, 12, and 15 nm, respectively (Figure 5b−d), which is consistent with the TGA results for the three composite samples. All of the carbon layers presented short-range-ordered amorphous structures.

The electrochemical lithium storage and cycling performances were investigated and compared for the different samples. Figure 6 presents typical charge/discharge curves of pristine Si, Si@C-1, Si@C-2, and Si@C-3 (third cycle) at a current rate of 0.3 A g^{-1}. As the carbon content increased, the voltage polarization became higher, which can be ascribed to the larger resistance to Li^+-ion transport due to the thicker carbon layers. The charge/discharge curves of pristine Si, Si@C-1, Si@C-2, and Si@C-3 at the 1st, 3rd, 30th, and 50th cycles are presented in Figure S3 (Supporting Information), and the corresponding differential capacity curves are presented in Figure S4 (Supporting Information). The initial discharge and charge capacities of the Si electrode were 3849.7 and 3279.0 mA h g^{-1}, respectively, with an initial Coulombic efficiency of 85.2%. Although pure Si exhibited the highest initial charge capacity, its capacity dropped quickly, and voltage polarization became very serious during cycling. In contrast, the capacity retention and electrochemical reversibility of the carbon coating samples improved, especially for Si@C-2. During 70 cycles, its specific capacity basically stabilized at ca. 1600 mA h g^{-1} (Figure 7a). A complete carbon layer with good electronic conductivity was found to suppress the particle volume change caused by the alloying of Li and Si and the Si side reaction with fluoride salt

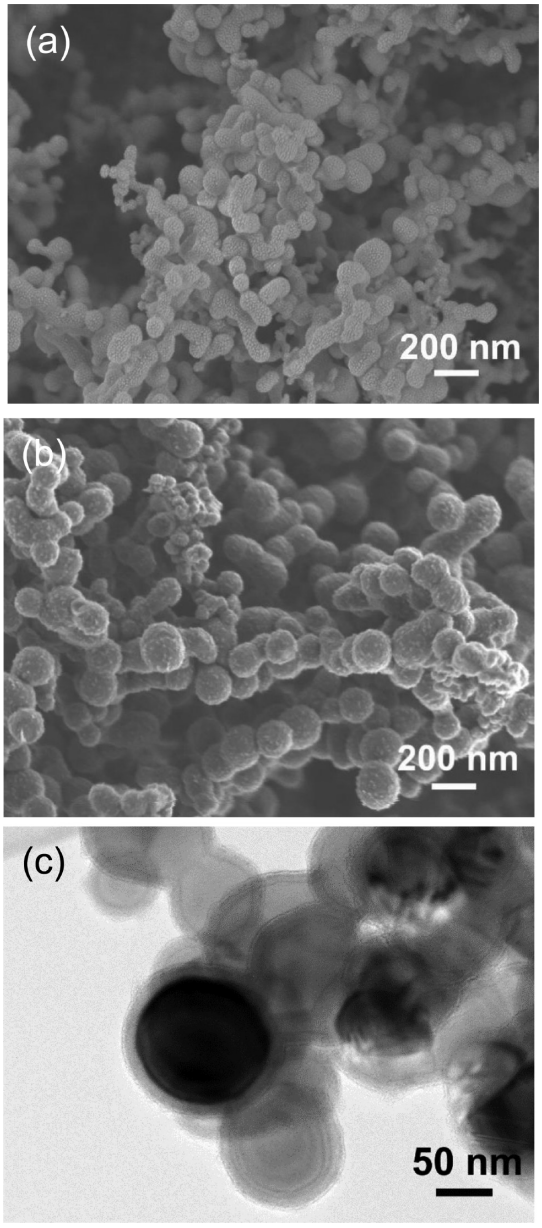

Figure 4. (a,b) SEM images of (a) pristine Si and (b) Si@C-2 and (c) TEM image of Si@C-2.

electrolyte, leading to a more stable conducting network in the electrode and interfacial properties. Thus, the electrochemical cycle reversibility was improved. The faster capacity fade for Si@C-1 in the initial cycle might be associated with a yet-insufficient volume buffering effect as a result of a carbon layer that was too thin. On the other hand, the high carbon content for Si@C-3 not only caused larger voltage polarization for charge/discharge, but also resulted in a relatively low cycle capacity (Figure 7a). The initial Coulombic efficiencies of Si@C-1, Si@C-2, and Si@C-3 were 83.6%, 80.1%, and 78.9%, respectively. The carbon coating thus decreased the Coulombic efficiency slightly. One reason for this behavior is that the carbon deposited from toluene by a CVD process has a very low Coulombic efficiency in the first cycle because of its amorphous structure, with a large number of defects that will trap and consume the intercalated lithium.[19,33] Therefore, a higher carbon content in the composite is related to a lower Coulombic efficiency. After 70 cycles, the Coulombic efficiency

dx.doi.org/10.1021/ie5010465 | Ind. Eng. Chem. Res. 2014, 53, 12697−12704

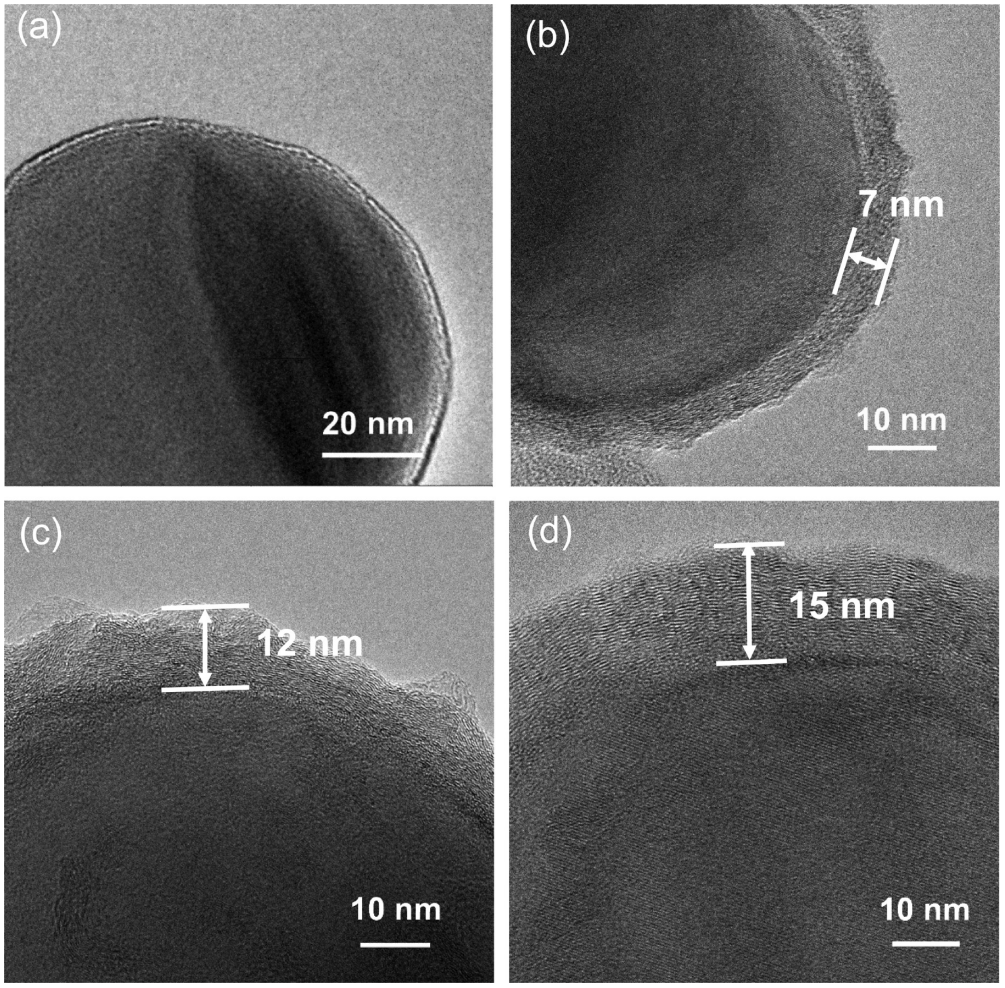

Figure 5. TEM images of (a) pristine Si, (b) Si@C-1, (c) Si@C-2, and (d) Si@C-3.

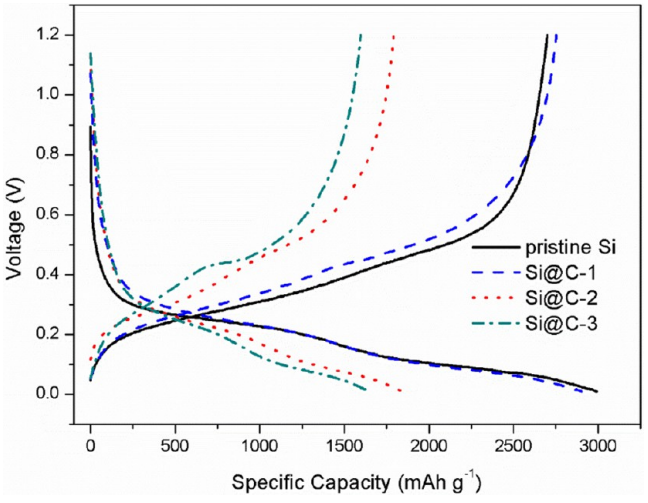

Figure 6. Typical charge/discharge profiles (third cycle) of coin cells with Si@C-1, Si@C-2, Si@C-3, and pristine Si at a current rate of 0.3 A g^{-1}.

of the carbon coating samples reached ca. 99.1%, whereas it was ca. 98.0% for pristine Si, indicating that the carbon coating was favorable for stabilizing the conductivity and SEI. Additionally, the first discharge curves of all samples displayed a long plateau below 0.15 V (Figure S3, Supporting Information), which corresponds to the Li-alloying process of crystalline Si to form an amorphous Li_xSi phase.[34] Afterward, the discharge and charge curves showed the characteristics of amorphous Si with an enhanced Li-insertion plateau. The detailed electrochemical alloying reactions for the different samples could be clearly characterized by the differential capacity curves in Figure S4 (Supporting Information). The first lithiation curves of pristine Si, Si@C-1, Si@C-2, and Si@C-3 showed sharp and strong peaks between 0.09 and 0.14 V, corresponding to the lithiation of crystalline Si into a $Li_{15}Si_4$ phase and/or amorphous Li_xSi alloy.[32,35] It is noteworthy that the first lithiation peak was shifted from 0.14 V (pristine Si) to 0.11 V (Si@C-1) and then further to 0.09 V (Si@C-2 and Si@C-3). This indicates that the carbon coating increased the voltage polarization. This is mainly related to the different SEIs for pristine Si and the carbon coating samples (i.e., Si/electrolyte and carbon/electrolyte interphases, respectively).[36] In addition, Li^+-ion transport across the resistant carbon layer is also responsible. The first delithiations of all of the samples showed a complicated peak character with a sharp peak at 0.42 V and a broad peak around 0.3 V, corresponding to delithiation from different Li_xSi phases.[32,35] The delithiation peak for carbon commonly observed at 0.2 V was too small to be visible, because of its small contribution to the overall capacity and the overlap of the broad peak around 0.3 V.[37] The subsequent cathodic and anodic curves of the samples showed two broad and weak peaks that are typical characteristics of lithiation and

dx.doi.org/10.1021/ie5010465 | Ind. Eng. Chem. Res. 2014, 53, 12697−12704

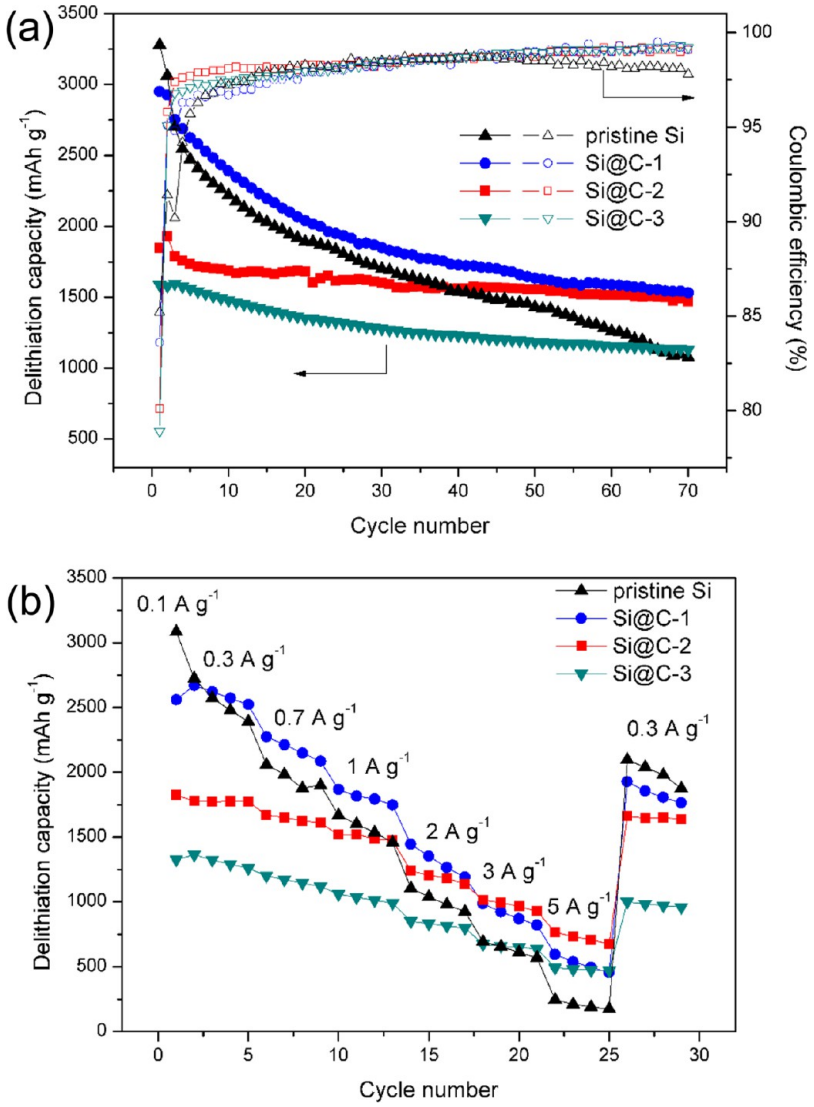

Figure 7. (a) Cycling performance and Coulombic efficiencies of Si@C-1, Si@C-2, Si@C-3, and pristine Si electrodes at a current rate of 0.3 A g^{-1} (first two cycles, 0.1 A g^{-1}). (b) Delithiation capacities of Si@C-1, Si@C-2, Si@C-3, and pristine Si cycled at different current rates from 0.1 to 5 A g^{-1}.

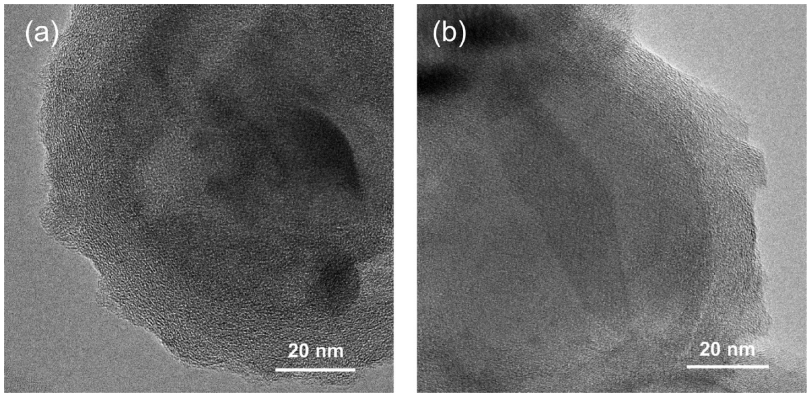

Figure 8. TEM images of Si@C-2 after the (a) 1st and (b) 30th cycles.

delithiation for amorphous Si.[32,38] Here, the peak positions and features varied significantly for the different samples, depending on the stability of the composite structure and its interface. The distance between the cathodic and anodic peaks, which is associated with the voltage polarization, increased for the pristine Si, but became steady for the Si samples with an adequately thick carbon layer.

The effect of the carbon layer thickness on the rate capability of the electrode was further examined by staged current rates from 0.1 to 5 A g^{-1}. As shown in Figure 7b, a delithiation

dx.doi.org/10.1021/ie5010465 | Ind. Eng. Chem. Res. 2014, 53, 12697−12704

capacity near 1770 mA h g^{-1} was obtained for the Si@C-2 electrode at a current rate of 0.3 A g^{-1}. The capacity declined regularly with increasing current rate. Even at the high current rate of 5 A g^{-1} (i.e., using 9 min for a complete charge or discharge process), the delithiation capacity of the Si@C-2 electrode was still around 750 mA h g^{-1}, twice the theoretical capacity of conventional graphite. In contrast, Si@C-1 and Si@C-3 delivered markedly lower capacities. For pristine Si, the capacity dropped dramatically from 2725 to 173 mA h g^{-1} when the current rate was increased from 0.3 to 5 A g^{-1}. The poor kinetic behavior of the Si electrode is attributed to the low electronic conductivity. On the other hand, the thick carbon layer for Si@C-3 might limit the fast transport of Li^+ ions. The above comparison indicates that the optimal carbon layer thickness on the Si surface is ca. 12 nm.

To further understand the superior cycling performance of Si@C-2, the stability of the carbon coating layer during cycling was examined by TEM and SEM. After each cycling test, the electrodes continued to be charged until reaching 2.2 V and were kept at 2.2 V for 3 h to fully delithiate the silicon. They were then washed with DMC to remove residual salt for SEM measurements and further soaked in water to remove the binder for TEM measurements. Figure 8 shows the TEM images of Si@C-2 composite after the 1st and 30th cycles. Even though the sample had been subjected to repeated lithium storage and ultrasonic pretreatments, the effective carbon coating on Si particles could still be observed. Moreover, the surface morphologies of the Si@C-2 electrode before and after 30 cycles were observed by SEM (Figure S5, Supporting Information). The particle features remained after the cycling test, but slight agglomeration and film covering were more obvious, indicating SEI film formation during cycling. This stable composite structure maintained good electronic conductivity and cycling reversibility. Iwamura et al. observed a different morphology evolution of nano-Si/C composites from spherical particles to wrinkled and netlike structures after 20 cycles.[32] This dramatic morphology change is difficult to explain in terms of the usual particle pulverization caused by the strong mechanical stress during lithium insertion and extraction. Another possible reason for the change in particle structure is the TEM sample preparation. This means that the TEM image might have been different from the actual state of the electrode. Unfortunately, their article did not describe the sample preparation for TEM characterization in detail. Actually, the cycled electrode contains various components, including Si, carbon black, binder, and electrolyte decomposition products similarly to the SEI. To disperse the nanoparticles well, the binder must be first removed. Incomplete delithiation after cycling can cause the reaction of the active particles with the water used for washing, leading to fragmentation and pulverization. In addition, the often-used strong ultrasonic treatment can also result in destruction of the structure of composite particles that have undergone full lithium insertion and extraction. Thus, a direct observation of the cycled electrode by SEM or other techniques could be helpful to confirm such a structure change.

Reaction temperatures of 700 and 900 °C for carbon deposition in the dynamic CVD process were also investigated with the same experimental conditions as used at 800 °C. It was found that toluene gas did not decompose to deposit a carbon layer on Si particles at 700 °C. The Si powder remained yellow at this temperature for a set time of 2 h, and no carbon layer could be observed by TEM. On the contrary, the toluene gas decomposed more quickly, and the carbon deposition rate was higher at 900 °C, compared with 800 °C. Thus, a shorter reaction time was needed for a similar carbon thickness. A sample obtained at 900 °C for 50 min (denoted as Si@C-900) shows a carbon layer thickness of ca. 11 nm (Figure S6a, Supporting Information), and a carbon content of 27.8% was determined by TGA, which was comparable to that of Si@C-2. The Raman spectra of these two samples are compared in Figure S6b (Supporting Information). Two typical carbon peaks can be observed: a disorder-induced D band (~1335 cm^{-1}) and a graphitic G band (~1585 cm^{-1}). The relative intensity ratio (i.e., R value) of the D and G bands is used to characterize the degree of disorder of carbon materials, and a larger R value indicates a higher degree of disorder.[39] The R values (I_D/I_G) of Si@C-2 and Si@C-900 were found to be 0.94 and 0.92, respectively, indicating similar carbon structural characteristics for Si@C-2 and Si@C-900. As shown in Figure S7 (Supporting Information), these two samples exhibited similar lithium storage capacities and cycling stabilities. However, a slight difference in the initial Coulombic efficiencies was found: 81.9% and 80.1% for Si@C-900 and Si@C-2, respectively. The efficiency enhancement for Si@C-900 is probably due not only to a lower amount of carbon but also to deeper carbonization and fewer defects at higher temperature.

On the other hand, acetylene as a carbon source was also found to be feasible for such a CVD process. However, obtaining a carbon coating using acetylene is more difficult than obtaining one using toluene, including safety issues. After 1.5 h at 800 °C, sample Si@C-ac with ca. 14.1% carbon was obtained. The TEM image in Figure S8a (Supporting Information) shows that the carbon layer on Si was ca. 6 nm. Because the carbon layer thickness and carbon content of Si@C-ac were close to those of Si@C-1, we compared these two samples. The TEM images indicate that they both presented typical short-layered structures of amorphous carbon, but the difference in carbon layer structures could hardly be distinguished. Figure S8b (Supporting Information) shows Raman spectra of the Si@C-1 and Si@C-ac composites. The R values of Si@C-1 and Si@C-ac were 0.89 and 0.99, respectively, indicating a more ordered carbon layer structure for Si@C-1. The effect of the carbon source on the electrochemical performance was also investigated. As shown in Figure 9, despite the similar initial delithiation capacities for the two samples, the cycling stability was significantly improved upon use of acetylene as the carbon source. Moreover, Si@C-ac demonstrated better rate performance than Si@C-1, although the capacities fell rapidly for both samples as the current rate was increased from 0.1 to 5 A g^{-1}. The obvious superiority of acetylene over toluene as the carbon source can be explained by the fact that the more ordered carbon planes of Si@C-1 could impede Li^+ ions from passing through the carbon layer. In addition, the more amorphous carbon layer can facilely endure the volume change of Si. In view of the advantages of acetylene as a carbon source, more detailed investigations should be done on the effect of the carbon layer thickness; the evolution of the interfacial properties during cycling; and the related CVD technology, including safety control and the ease of adjustment of the carbon layer thickness.

4. CONCLUSIONS

In summary, we have employed a facile and dynamic CVD process to coat a uniform carbon nanolayer on Si particles. When toluene is used as the carbon source, the carbon layer

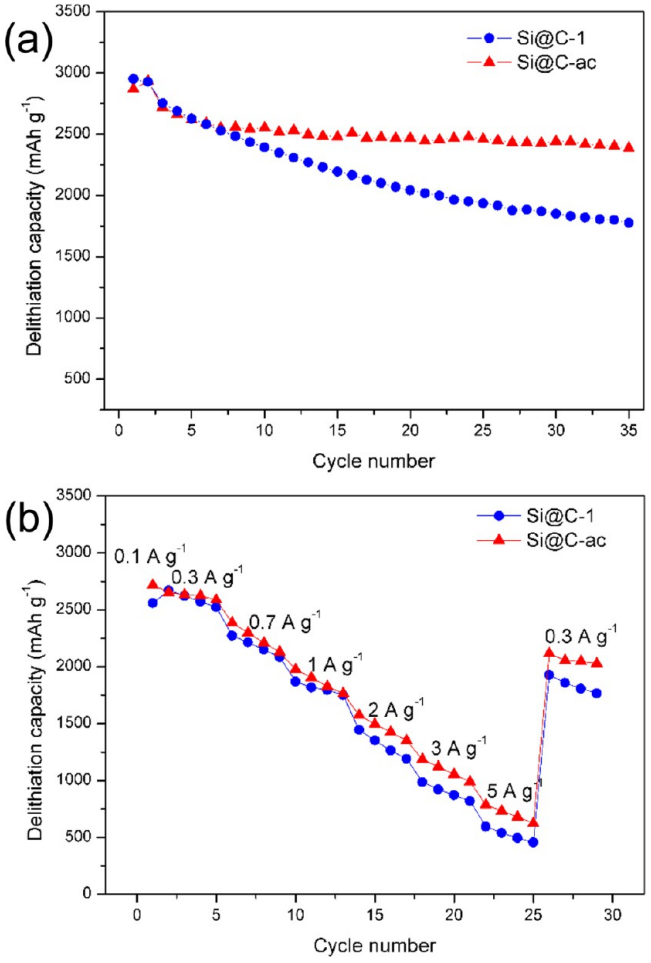

Figure 9. (a) Cycling performance (first two cycles, 0.1 A g^{-1}; subsequent cycles, 0.3 A g^{-1}) and (b) rate performance of Si@C-1 and Si@C-ac.

thickness can be effectively controlled by the CVD reaction time under a fixed precursor gas flux. The resulting Si@C composites were examined as the anode material for LIBs. It was found that the carbon layer thickness greatly influences the specific capacity, cycle stability, and high-rate capability. The optimal Si@C composite with a carbon layer of ca. 12 nm showed a fairly stable capacity of about 1600 mA h g^{-1} during 70 cycles at 0.3 A g^{-1}. A large capacity of ca. 750 mA h g^{-1} was available even at the high current rate of 5 A g^{-1}. The significant improvement in the electrochemical performance obtained by applying a carbon coating on Si can be attributed to the suppressed volume effect, improved electronic conductivity, and stable composite structure upon cycling. On the other hand, it should be mentioned that the effect of the carbon source on the electrochemical performance of the carbon-coated Si was also found to be notable. The primary results showed that acetylene is superior to toluene as a carbon source. A possible reason for this difference is that a more amorphous carbon layer could facilitate the movement of Li^+ ions across the carbon layer and accommodate the volume change of Si. Overall, the dynamic CVD technology is suitable for the large-scale fabrication of coated or modified composite materials for battery and other applications.

■ ASSOCIATED CONTENT

Supporting Information

Photograph of the quartz tube of the CVD furnace; TGA curves of samples from different locations in the tube; charge/discharge profiles and corresponding differential capacity curves of pristine Si, Si@C-1, Si@C-2, and Si@C-3 at different cycles; SEM images of Si@C-2 electrode before and after cycling; TEM images of Si@C-900 and Si@C-ac; Raman spectra of Si@C-2, Si@C-900, Si@C-1, and Si@C-ac; and cycling performances of Si@C-2 and Si@C-900. This material is available free of charge via the Internet at http://pubs.acs.org.

■ AUTHOR INFORMATION

Corresponding Author

*Tel.: +86-21-54747667. Fax: +86-21-54747667. E-mail: yangj723@sjtu.edu.cn.

Notes

The authors declare no competing financial interest.

■ ACKNOWLEDGMENTS

We are grateful for the financial support of this work by the National Key Basic Research Program of China (No. 2014CB932303) and the SJTU-UM Joint Research Project.

■ REFERENCES

(1) Tarascon, J.-M.; Armand, M. Issues and challenges facing rechargeable lithium batteries. *Nature* **2001**, *414*, 359−367.
(2) Armand, M.; Tarascon, J.-M. Building better batteries. *Nature* **2008**, *451*, 652−657.
(3) Bruce, P. G.; Scrosati, B.; Tarascon, J. M. Nanomaterials for rechargeable lithium batteries. *Angew. Chem., Int. Ed.* **2008**, *47*, 2930−2946.
(4) Endo, M.; Kim, C.; Nishimura, K.; Fujino, T.; Miyashita, K. Recent development of carbon materials for Li ion batteries. *Carbon* **2000**, *38*, 183−197.
(5) Besenhard, J.; Yang, J.; Winter, M. Will advanced lithium-alloy anodes have a chance in lithium-ion batteries? *J. Power Sources* **1997**, *68*, 87−90.
(6) Huggins, R. A. Lithium alloy negative electrodes. *J. Power Sources* **1999**, *81*, 13−19.
(7) Wu, H.; Cui, Y. Designing nanostructured Si anodes for high energy lithium ion batteries. *Nano Today* **2012**, *7*, 414−429.
(8) Yu, Y.; Gu, L.; Zhu, C.; Tsukimoto, S.; van Aken, P. A.; Maier, J. Reversible Storage of Lithium in Silver-Coated Three-Dimensional Macroporous Silicon. *Adv. Mater.* **2010**, *22*, 2247−2250.
(9) Wang, C.; Wu, H.; Chen, Z.; McDowell, M. T.; Cui, Y.; Bao, Z. Self-healing chemistry enables the stable operation of silicon microparticle anodes for high-energy lithium-ion batteries. *Nat. Chem.* **2013**, *5*, 1042−1048.
(10) Beaulieu, L.; Eberman, K.; Turner, R.; Krause, L.; Dahn, J. Colossal reversible volume changes in lithium alloys. *Electrochem. Solid-State Lett.* **2001**, *4*, A137−A140.
(11) Liu, H. K.; Guo, Z.; Wang, J.; Konstantinov, K. Si-based anode materials for lithium rechargeable batteries. *J. Mater. Chem.* **2010**, *20*, 10055−10057.
(12) Chan, C. K.; Peng, H.; Liu, G.; McIlwrath, K.; Zhang, X. F.; Huggins, R. A.; Cui, Y. High-performance lithium battery anodes using silicon nanowires. *Nat. Nanotechnol.* **2008**, *3*, 31−35.
(13) Choi, J. W.; McDonough, J.; Jeong, S.; Yoo, J. S.; Chan, C. K.; Cui, Y. Stepwise nanopore evolution in one-dimensional nanostructures. *Nano Lett.* **2010**, *10*, 1409−1413.
(14) Park, M.-H.; Kim, M. G.; Joo, J.; Kim, K.; Kim, J.; Ahn, S.; Cui, Y.; Cho, J. Silicon nanotube battery anodes. *Nano Lett.* **2009**, *9*, 3844−3847.
(15) Song, T.; Xia, J.; Lee, J.-H.; Lee, D. H.; Kwon, M.-S.; Choi, J.-M.; Wu, J.; Doo, S. K.; Chang, H.; Park, W. I. Arrays of sealed silicon

nanotubes as anodes for lithium ion batteries. *Nano Lett.* **2010**, *10*, 1710−1716.
(16) Wu, H.; Chan, G.; Choi, J. W.; Ryu, I.; Yao, Y.; McDowell, M. T.; Lee, S. W.; Jackson, A.; Yang, Y.; Hu, L. Stable cycling of double-walled silicon nanotube battery anodes through solid-electrolyte interphase control. *Nat. Nanotechnol.* **2012**, *7*, 310−315.
(17) Iwamura, S.; Nishihara, H.; Kyotani, T. Effect of Buffer Size around Nanosilicon Anode Particles for Lithium-Ion Batteries. *J. Phys. Chem. C* **2012**, *116*, 6004−6011.
(18) Kim, H.; Seo, M.; Park, M. H.; Cho, J. A Critical Size of Silicon Nano-Anodes for Lithium Rechargeable Batteries. *Angew. Chem., Int. Ed.* **2010**, *49*, 2146−2149.
(19) Jia, H.; Gao, P.; Yang, J.; Wang, J.; Nuli, Y.; Yang, Z. Novel Three-Dimensional Mesoporous Silicon for High Power Lithium-Ion Battery Anode Material. *Adv. Energy Mater.* **2011**, *1*, 1036−1039.
(20) Feng, X.; Yang, J.; Gao, P.; Wang, J.; Nuli, Y. Facile approach to an advanced nanoporous silicon/carbon composite anode material for lithium ion batteries. *RSC Adv.* **2012**, *2*, 5701−5706.
(21) Jung, D. S.; Hwang, T. H.; Park, S. B.; Choi, J. W. Spray Drying Method for Large-Scale and High-Performance Silicon Negative Electrodes in Li-Ion Batteries. *Nano Lett.* **2013**, *13*, 2092−2097.
(22) Gao, P.; Fu, J.; Yang, J.; Lv, R.; Wang, J.; Nuli, Y.; Tang, X. Microporous carbon coated silicon core/shell nanocomposite via in situ polymerization for advanced Li-ion battery anode material. *Phys. Chem. Chem. Phys.* **2009**, *11*, 11101−11105.
(23) Guan, H.; Wang, X.; Chen, S.; Bando, Y.; Golberg, D. Coaxial Cu−Si@C array electrodes for high-performance lithium ion batteries. *Chem. Commun.* **2011**, *47*, 12098−12100.
(24) Liu, W.-R.; Wang, J.-H.; Wu, H.-C.; Shieh, D.-T.; Yang, M.-H.; Wu, N.-L. Electrochemical characterizations on Si and C-coated Si particle electrodes for lithium-ion batteries. *J. Electrochem. Soc.* **2005**, *152*, A1719−A1725.
(25) Cakan, R. D.; Titirici, M.-M.; Antonietti, M.; Cui, G.; Maier, J.; Hu, Y.-S. Hydrothermal carbon spheres containing silicon nanoparticles: Synthesis and lithium storage performance. *Chem. Commun.* **2008**, *32*, 3759−3761.
(26) Feng, X.; Yang, J.; Lu, Q.; Wang, J.; Nuli, Y. Facile approach to SiO_x/Si/C composite anode material from bulk SiO for lithium ion batteries. *Phys. Chem. Chem. Phys.* **2013**, *15*, 14420−14426.
(27) Xiao, J.; Xu, W.; Wang, D.; Choi, D.; Wang, W.; Li, X.; Graff, G. L.; Liu, J.; Zhang, J.-G. Stabilization of Silicon Anode for Li-Ion Batteries. *J. Electrochem. Soc.* **2010**, *157*, A1047−A1051.
(28) Si, Q.; Hanai, K.; Ichikawa, T.; Phillipps, M.; Hirano, A.; Imanishi, N.; Yamamoto, O.; Takeda, Y. Improvement of cyclic behavior of a ball-milled SiO and carbon nanofiber composite anode for lithium-ion batteries. *J. Power Sources* **2011**, *196*, 9774−9779.
(29) Yang, J.; Wang, B.; Wang, K.; Liu, Y.; Xie, J.; Wen, Z. Si/C composites for high capacity lithium storage materials. *Electrochem. Solid-State Lett.* **2003**, *6*, A154−A156.
(30) Wen, Y.; Zhu, Y.; Langrock, A.; Manivannan, A.; Ehrman, S. H.; Wang, C. Graphene-Bonded and -Encapsulated Si Nanoparticles for Lithium Ion Battery Anodes. *Small* **2013**, *9*, 2810−2816.
(31) Yoshio, M.; Wang, H.; Fukuda, K.; Umeno, T.; Dimov, N.; Ogumi, Z. Carbon-Coated Si as a Lithium-Ion Battery Anode Material. *J. Electrochem. Soc.* **2002**, *149*, A1598−A1603.
(32) Iwamura, S.; Nishihara, H.; Kyotani, T. Fast and reversible lithium storage in a wrinkled structure formed from Si nanoparticles during lithiation/delithiation cycling. *J. Power Sources* **2013**, *222*, 400−409.
(33) Yen, Y.-C.; Chao, S.-C.; Wu, H.-C.; Wu, N.-L. Study on solid-electrolyte-interphase of Si and C-coated Si electrodes in lithium cells. *J. Electrochem. Soc.* **2009**, *156*, A95−A102.
(34) McDowell, M. T.; Lee, S. W.; Nix, W. D.; Cui, Y. 25th Anniversary Article: Understanding the Lithiation of Silicon and Other Alloying Anodes for Lithium-Ion Batteries. *Adv. Mater.* **2013**, *25*, 4966−4985.
(35) Obrovac, M.; Christensen, L. Structural changes in silicon anodes during lithium insertion/extraction. *Electrochem. Solid-State Lett.* **2004**, *7*, A93−A96.
(36) Ng, S. H.; Wang, J.; Wexler, D.; Chew, S. Y.; Liu, H. K. Amorphous Carbon-Coated Silicon Nanocomposites: A Low-Temperature Synthesis via Spray Pyrolysis and Their Application as High-Capacity Anodes for Lithium-Ion Batteries. *J. Phys. Chem. C* **2007**, *111*, 11131−11138.
(37) Magasinski, A.; Dixon, P.; Hertzberg, B.; Kvit, A.; Ayala, J.; Yushin, G. High-performance lithium-ion anodes using a hierarchical bottom-up approach. *Nat. Mater.* **2010**, *9*, 353−358.
(38) Obrovac, M.; Krause, L. Reversible cycling of crystalline silicon powder. *J. Electrochem. Soc.* **2007**, *154*, A103−A108.
(39) Fu, K.; Xue, L.; Yildiz, O.; Li, S.; Lee, H.; Li, Y.; Xu, G.; Zhou, L.; Bradford, P. D.; Zhang, X. Effect of CVD carbon coatings on Si@CNF composite as anode for lithium-ion batteries. *Nano Energy* **2013**, *2*, 976−986.